Plasma Amino Acid Coatings for a Conformal Growth of Titania Nanoparticles

Kyle D. Anderson,[†] Kamil Marczewski,[†] Srikanth Singamaneni,[†] Joseph M. Slocik,[‡] Rachel Jakubiak,[‡] Rajesh R. Naik,[‡] Timothy J. Bunning,[‡] and Vladimir V. Tsukruk*,[†]

School of Materials Science and Engineering, Georgia Institute of Technology, Atlanta, Georgia 30332, and Materials and Manufacturing Directorate, Air Force Research Laboratory, Wright-Patterson Air Force Base, Dayton, Ohio 45433-7702

ABSTRACT We report on the conformal synthesis of ultrathin films from the aminoacid histidine on flat silicon substrates and 3D periodic polymer structures via plasma enhanced chemical vapor deposition. We demonstrate the efficient utilization of this functional amino acid nanocoating for the formation of individual titania nanoparticles with dimensions from 2 to 15 nm depending upon reduction conditions. The titania nanoparticles were grown directly on histidine-functionalized planar and 3D polymer substrates by a wet-chemistry method that showed uniform surface coverage that reached approximately 75%. This approach demonstrates the potential for modifying the optical properties of periodic porous polymeric structures via direct conformal growth of titania nanoparticles.

KEYWORDS: plasma-enhanced chemical vapor deposition • titania nanoparticles • histidine coatings • conformal modification

INTRODUCTION

Surface functionalization is frequently used to alter or enhance the desired response in organized organic and inorganic structures in order to tailor their optical properties, reactivity, mechanical strength, surface wettability, biocompatibility, sensing ability, and photovoltaic capability (1–10). Some systems currently studied make use of the active sites on biological molecules, which supports the reduction of inorganic compounds directly from solution onto the surface (11–14). This approach allows the direct modification of surface properties through tailored wet-chemistry nanoparticle reduction from precursor solutions on properly functionalized substrates. On the basis of these systems, new bottom-up techniques can be developed for material fabrication or surface enhancement via surface protein and peptide mediated synthesis (15–19).

Mimicking a naturally occurring biomineralization process has promising implications for biomimetic engineering. A variety of different metal-binding synthetic macromolecules, proteins, and peptides have been demonstrated to effectively form inorganic nanoparticles from precursor solutions and bind them to functionalized surfaces where an excess of the protein or amino acid is properly tethered (20). Functionalized polymeric materials, such as poly(ethyleneimine) and multifunctional hyperbranched molecules, have been demonstrated to be effective in the reduction of silver and gold nanoparticles as well (21, 22).

Many examples of this bioenabled approach have been demonstrated, including but not limited to the use of biological and synthetic macromolecules containing tyrosine, tryptophan, and cysteine groups for the controlled formation of gold nanostructures; tyrosine, AG3 &AG4 peptides for the reduction of silver nanoparticles; and cysteine for obtaining platinum nanostructures, to name only a few examples (15, 23–27). As known, proteins and peptides with higher concentrations of charged amino acids (e.g., arginine, lysine) are effective in the reduction of titania nanoparticles (28–31). Additionally, histidine aminoacids with their high concentration of amine groups are considered to be potential precursors for titania reduction, enabling nanoparticle formation from aqueous solution onto the surfaces (15, 32). The rSilC protein is one such class that has been demonstrated as being effective at functionalizing surfaces for the formation of large titania structures and nanoparticles in both bulk solution and at surfaces (33, 34).

In our studies, we focus on developing the potential of direct growth of the inorganic phase as a method to modify the optical properties of polymer substrates and periodic structures by the in situ growth of high-refractive index materials. This may enable optically active polymeric stacks which might possess a high contrast in refractive index. Using an active layer for the nanoparticle reduction enables the prospective high-refractive index material to be grown directly on the final configuration. Many previous studies have used high refractive index materials, such as titania, in one dimensional photonic structures because of the large refractive index it affords compared with many other materials (35–39). Various methods including atomic layer deposition, chemical vapor deposition, sol−gel process, and electrodeposition have all been employed to create inorganic conformal nanocoatings (40–42). However, most of these

* Corresponding author. Tel: (404) 894-6081. Fax: (404) 385-3112. E-mail: vladimir@mse.gatech.edu.
Received for review April 16, 2010 and accepted June 29, 2010
[†] Georgia Institute of Technology.
[‡] Air Force Research Laboratory.
DOI: 10.1021/am1003365

Report Documentation Page

Form Approved
OMB No. 0704-0188

1. REPORT DATE	2. REPORT TYPE	3. DATES COVERED
APR 2010		**00-00-2010 to 00-00-2010**

4. TITLE AND SUBTITLE	5a. CONTRACT NUMBER
Plasma Amino Acid Coatings for a Conformal Growth of Titania Nanoparticles	5b. GRANT NUMBER
	5c. PROGRAM ELEMENT NUMBER
6. AUTHOR(S)	5d. PROJECT NUMBER
	5e. TASK NUMBER
	5f. WORK UNIT NUMBER
7. PERFORMING ORGANIZATION NAME(S) AND ADDRESS(ES) **Georgia Institute of Technology,School of Materials Science and Engineering,Atlanta,GA,30332**	8. PERFORMING ORGANIZATION REPORT NUMBER
9. SPONSORING/MONITORING AGENCY NAME(S) AND ADDRESS(ES)	10. SPONSOR/MONITOR'S ACRONYM(S)
	11. SPONSOR/MONITOR'S REPORT NUMBER(S)

12. DISTRIBUTION/AVAILABILITY STATEMENT
Approved for public release; distribution unlimited

13. SUPPLEMENTARY NOTES

14. ABSTRACT

We report on the conformal synthesis of ultrathin films from the aminoacid histidine on flat silicon substrates and 3D periodic polymer structures via plasma enhanced chemical vapor deposition. We demonstrate the efficient utilization of this functional amino acid nanocoating for the formation of individual titania nanoparticles with dimensions from 2 to 15 nm depending upon reduction conditions. The titania nanoparticles were grown directly on histidine-functionalized planar and 3D polymer substrates by a wet-chemistry method that showed uniform surface coverage that reached approximately 75%. This approach demonstrates the potential for modifying the optical properties of periodic porous polymeric structures via direct conformal growth of titania nanoparticles.

15. SUBJECT TERMS

16. SECURITY CLASSIFICATION OF:			17. LIMITATION OF ABSTRACT	18. NUMBER OF PAGES	19a. NAME OF RESPONSIBLE PERSON
a. REPORT **unclassified**	b. ABSTRACT **unclassified**	c. THIS PAGE **unclassified**	**Same as Report (SAR)**	**13**	

Scheme 1. The Fabrication Process Beginning with Sublimation of Histidine Amino Acid, Followed by Immersion into Precursor Solution, and Resulting in Growth of Titania Nanoparticles[a]

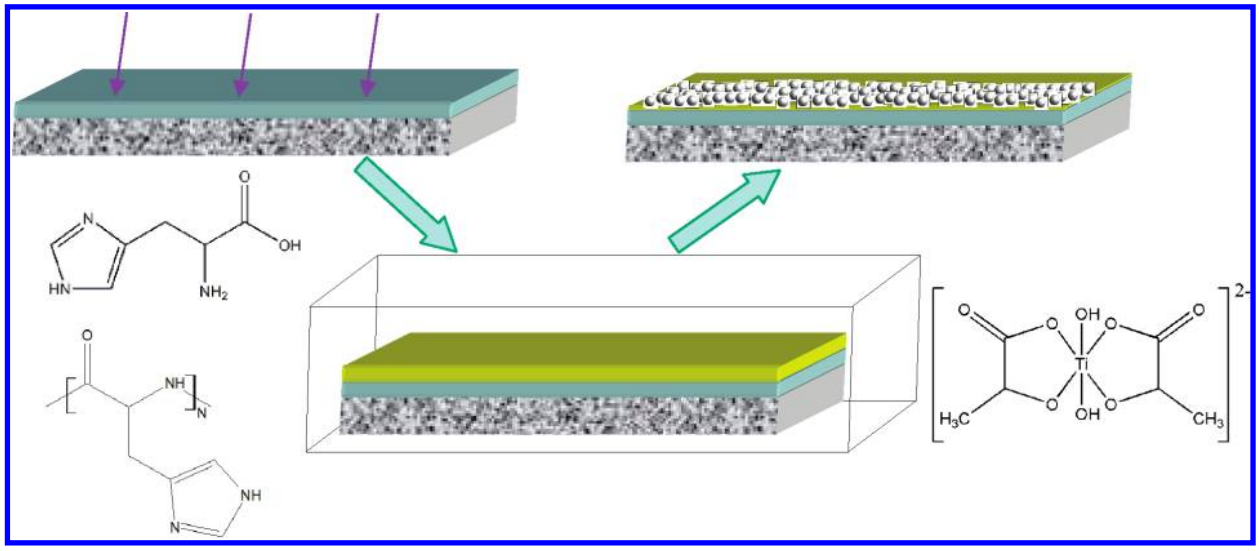

[a] The chemical structures of histidine (left top), polyhistidine (left bottom) and TiBAHLD pre-cursor (right) are shown as well.

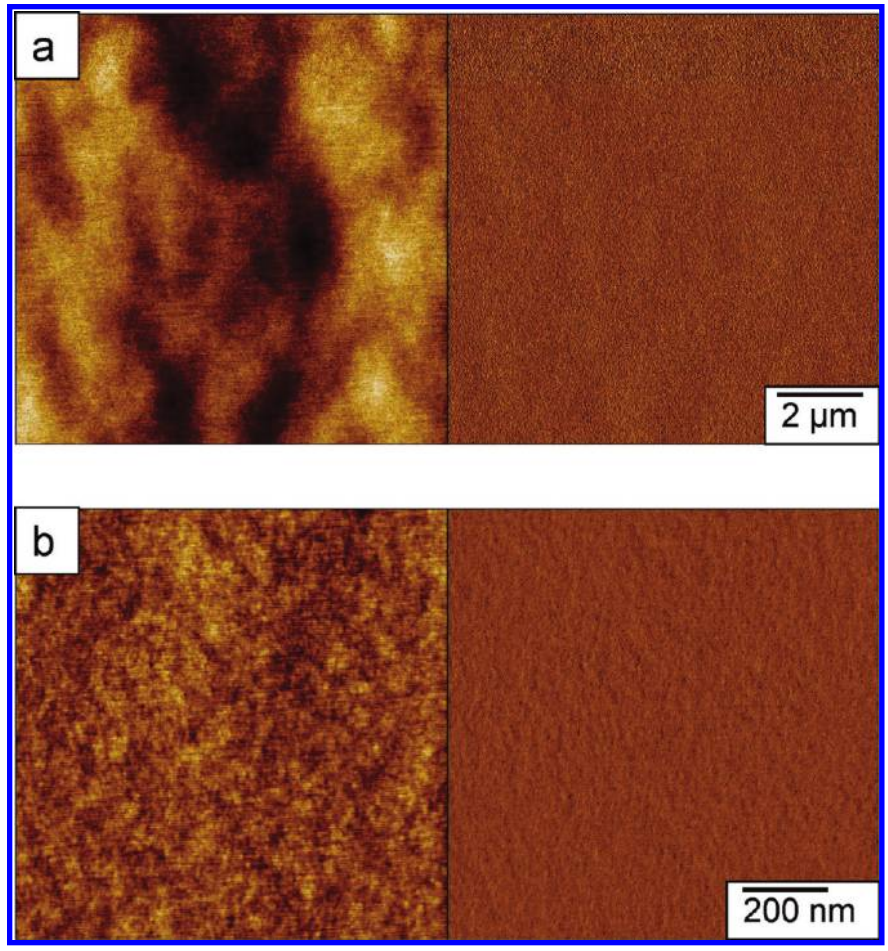

FIGURE 1. Model plasma-polymerized histidine films deposited on silicon wafers show smooth and uniform surface morphology. AFM images show topography (left) and phase (right) at different magnifications (both images) with (a) $z = 5$ nm height and 10° phase and (b) $z = 3$ nm height and 10° phase.

techniques either require high temperatures, result in incomplete filling or clogging of the structures, or promote their disintegration and collapse.

In this study, we exploit a synthetic histidine monomer for the fabrication of robust and uniform nanocoatings capable of forming titania nanostructures on different sub-

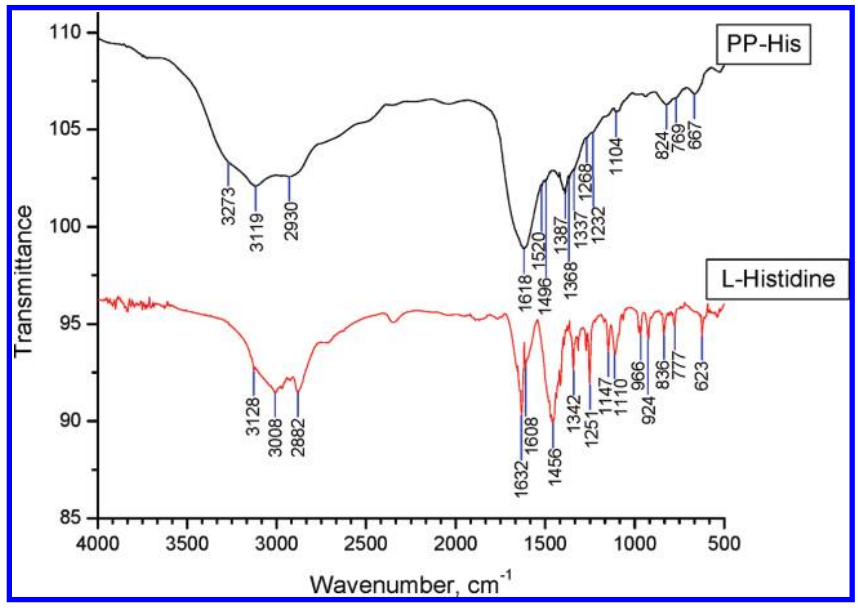

FIGURE 2. FTIR spectra of L-histidine monomer and plasma-polymerized PP-his films.

Table 1. FTIR Peak Positions and Assignments for PP-His and L-Histidine Films[a]

PP-His			L-histidine			polyhistidine
3273	w	N−H backbone				3282
3119	m	N−H	3127	m	OH-O hydrogen bond, N−H	3075
			3008	**s**	C═C aromatic	2972
2930	w	C−H				
			2882	**s**	C−H aliphatic stretch	**2895**
1618	**s**	C═O, C═N backbone	**1632**	**s**	C═O stretch, NH2	**1642**
			1608	m	NH_2, C═N	
						1574
						1545
1520	w	H−N−C backbone				1510
			1456	s	COOH stretching	**1446**
						1433
						1401
1368	w	H−N−C, C−N, C═C, H−N═C, N═C−H, C−N				1362
1337	w	H−C═C, H−N−C, N−C−H, C−N, H−N−C, H−N═C	1342	m	CH2 twist	1330
1268	w	C═N, H−C−C, C═O, C−C−H, N−C, H−C−C, C−C				
1232	w	C═N, H−C−C, C−C, C−C−H, C═O, C−C	**1251**	**s**	COOH	**1230**
			1147	m	CH or NH deformation	
1104	m	C−N,H−C-C, C−C, N−C−H, C═N, C−N, C−C═C	1110	m	O−H.. .O in plane bend	1112
						1085
			966	w	ring sym stretch	988
824	m	C−C, C−N, C═C, C−N═C, C−N	836	m	ring sym stretch, H wag	827
769	w	C═O, N−H backbone	777	m	C═O	767
						754
						689
667	**s**	C−N−C, N═C−N, H−N−C, C−N, C−N═C, C═C−N	**623**	**s**	**ring deformation**	**662**
						564
						546

[a] Peaks reported in literature for synthetic polyhistidine are included for reference from (61).

strates. We utilized a plasma-enhanced chemical vapor deposition (PECVD) technique which has proven to be a reliable method for creating ultrathin robust coatings quickly and over a large area while retaining functionality (43–45). Our recent work has shown that PECVD is well-suited for the sublimation of powdered amino acids and their deposition on target substrates in the form of crosslinked nanocoatings (46, 47). Using a similar process here, we extend that capability with the demonstration of plasma polymerized histidine for the reduction of titania nanoparticles onto both flat substrates and periodic porous polymeric structures (48–50). We demonstrate the formation of uniform indi-

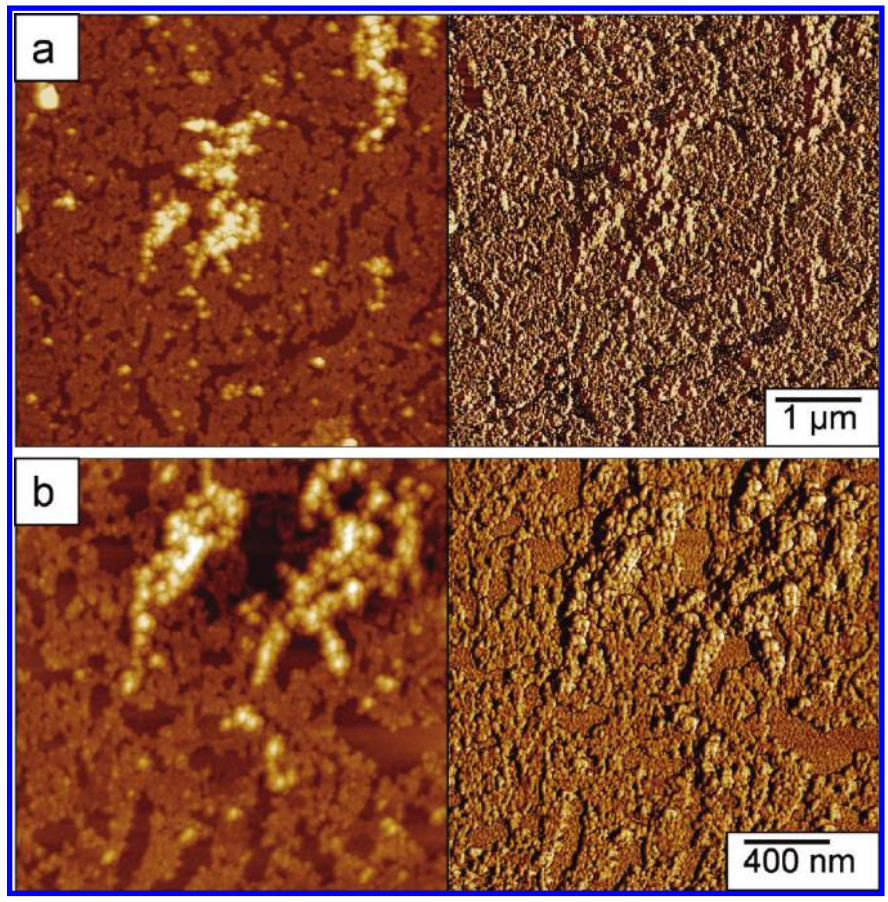

FIGURE 3. AFM images (topography, left; phase, right) of plasma polymerized histidine film with titania nanoparticles formed from aqueous precursor solution; $z = 75$ nm height and 40° phase for all images.

vidual titania nanoparticles on a plasma deposited histidine nanocoatings on both smooth substrates and in a highly conformal manner on periodic porous polymer structures fabricated by interference lithography.

EXPERIMENTAL SECTION

Synthetic amino acid monomer, L-histidine (Sigma), was purchased and used without further modification for all plasma depositions. Depositions were performed on highly polished single-crystal {100} silicon wafers cleaned in piranha solution (3:1 Conc. H_2SO_4 and 30% H_2O_2) for 1 h and then rinsed with Nanopure water (18 MΩ cm). A custom built plasma chamber used a capacitively coupled RF power source (13.56 MHz) to generate the plasma. A temperature of approximately 200 °C was applied to the L-histidine monomer and then slightly reduced, once sublimation had begun in order to sustain the heating while giving the monomer a longer time to sublime. The histidine amino acid was in powder form and was placed in a tantalum heating boat in the PECVD chamber and kept under high vacuum for 20 min prior to deposition. All histidine sublimation procedures were carried out according to the well-established routine with chamber pressure of 0.02 Torr, Argon (99.99% purity) flow rate of 10 cm^3/min and RF power applied at 50 W (46, 51, 52).

The fabrication process is shown in Scheme 1 along with chemical structures of the compounds used in this study. The dry histidine monomer was deposited in a custom built plasma chamber through the direct sublimation of the solid monomer into the plasma stream (46). As the dry monomer was heated and sublimed into the plasma stream, smooth, conformal films were formed on the substrates. All substrates were placed perpendicular to the plasma stream and were rotated to ensure uniform coverage during the deposition. Upon removal from the plasma chamber, the plasma polymerized histidine (PP-His) coated substrate was immersed in a titanium(IV) bis-(ammonium lactate) dihydroxide (TiBALDH) solution to allow mineralization to occur. After removal of the substrate from the TiBALDH, it was rinsed with Nanopure water and dried under nitrogen.

A 2 M TiBALDH solution of was purchased from Aldrich and used for all particle reduction experiments. The TiBALDH solution for mineralization was prepared by diluting this into two separate solutions, one with buffer and one with Nanopure water. 0.5 M phosphate citrate buffer was prepared and used at pH 7 to dilute the TiBALDH to a final concentration of 2 mM. Both solutions (water and buffer) were mixed at a 3:500 volume ratio and mixed thoroughly before the histidine coated wafers were immersed. Samples were exposed to the solution for different lengths of time ranging from 1 to 24 h and then removed, rinsed twice, and dried under a stream of dry nitrogen. Periodic porous polymer SU8 templates fabricated using multi-beam IL according to published procedures have been supplied by Thomas lab (48). The materials platform consisted of Epon-SU8 (Miller Stephensen) as a photoresist (a multi-functional epoxy derivative of a bisphenol-A Novolac) and H-Nu 470 (Spectra group) as a photosensitizer (53, 54).

Atomic force microscopy (AFM) images at different magnifications were taken using Dimension 3000 and MultiMode microscopes, both with a Nanoscope IIIa controller utilizing a light tapping regime in accordance with established procedures (55–57). Aluminum backed triangle silicon cantilevers (Mikro-Masch) with a nominal spring constant of 40 N m^{-1} were used for all measurements. X-ray photoelectron spectroscopy (XPS)

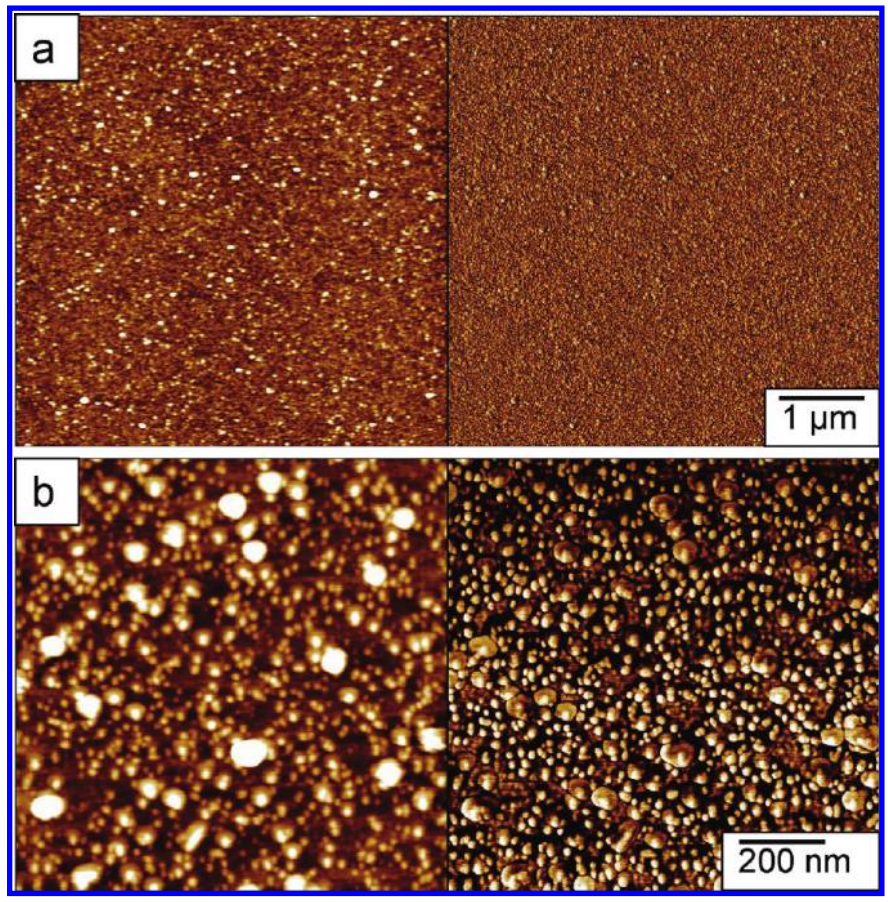

FIGURE 4. AFM images (topography, left; phase, right) of histidine film with titania nanoparticles formed on PP-His in phosphate citrate buffer for 24 h; (a) $z = 10$ nm height and 30° phase. (b) $z = 6$ nm height and 10° phase.

measurements were performed using an M-PROBE Surface Science XPS spectrometer utilizing charge neutralization. Spectra were collected from 0−1000 eV at 1 eV steps at a spot size of 800 μm and averaged over 15 scans for standard resolution and from 450−470 eV at 0.1 eV steps for high resolution.

Optical characterization of aminoacid coatings before and after titania formation was carried out with a Woollam M2000U multiangle spectroscopic ellipsometer with measurements at three different angles: 65, 70, and 75°. The optical constants n (refractive index) and k (absorbance) were determined using both the Cauchy model and Effective Medium Approximation (EMA) over the range of wavelengths $\lambda = 250$ nm to 1000 nm. Fourier transform IR spectra (FTIR) measurements were conducted on a Perkin-Elmer SPECTRUM 2000 FT-IR spectrometer in transmission mode. Samples were prepared on double sided polished silicon wafers to minimize the background signal.

Raman measurements were performed using a Witec (Alpha 300R) confocal Raman microscope using Ar+ ion laser (514.5 nm) as an excitation source. The intensity of the excitation source was fixed at 1 mW. Silver nanoparticles (12 nm) were used to provide surface enhancement on the PP-His coated silicon wafers.

RESULTS AND DISCUSSION

Plasma-Polymerized Histidine Films. The PP-His deposited film was seen to be smooth and pinhole free with a surface microroughness of 0.3 nm over a 1x1μm^2 surface area (Figure 1). This histidine film morphology is similar to plasma polymerized ultrathin films from various monomers showing smooth, defect free structures which uniformly coat the target surface. At higher magnification, a very fine grainy texture is observed which is a characteristic surface feature of plasma polymerized films with a random cross-linked network of polymerized segments (47, 51).

The thickness of the film within 150−200 nm was controlled through the deposition time and the amount of material used. The films did not delaminate from the substrate upon removal from the plasma chamber and subsequent exposure to air. The plasma polymerized histidine films were also stable under light mechanical abrasion and showed good adhesion to the substrate. However, the PP-His films did not show the same robustness when immersed in water as they tended to partially dissolve, indicating there may be not complete network formation occurring. A very thin (few nanometers) residual surface layer of histidine is preserved after exposure to the precursor solution thus facilitating further titania forming routines.

After plasma deposition of the histidine, the resulting chemical structure was compared to a solution-cast film of histidine to verify if the PP-His film retained functional groups necessary for titania formation, namely the amine functional groups (Figure 2). FTIR spectra show that key functional groups are retained after the polymerization process but there are some notable differences indicating that significant chemical changes occur (see peak positions and assignments in Table 1) (62, 58–60). Although, most major peaks of the initial histidine monomer can be found in the FTIR spectrum of PP-His, they are much broader and

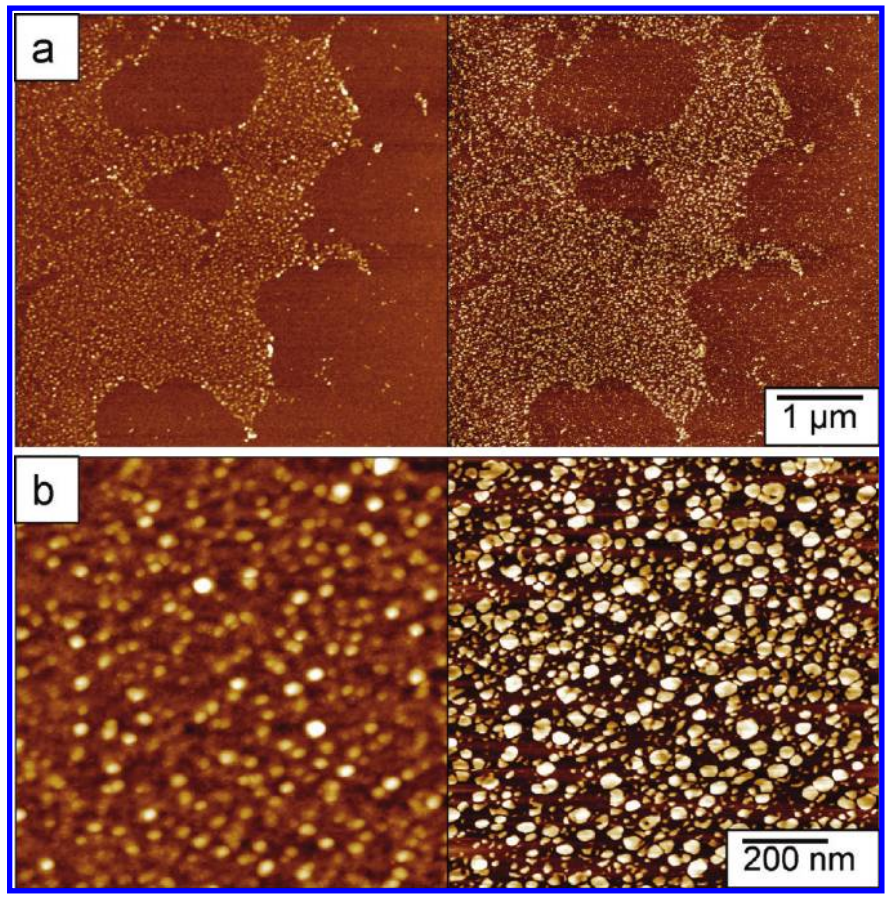

FIGURE 5. AFM images (topography, left; phase, right) of histidine film with TiO_2 nanoparticles formed on PP-His in phosphate citrate buffer for 2 h; (a) $z = 20$ nm height and 100° phase. (b) $z = 15$ nm height and 70° phase.

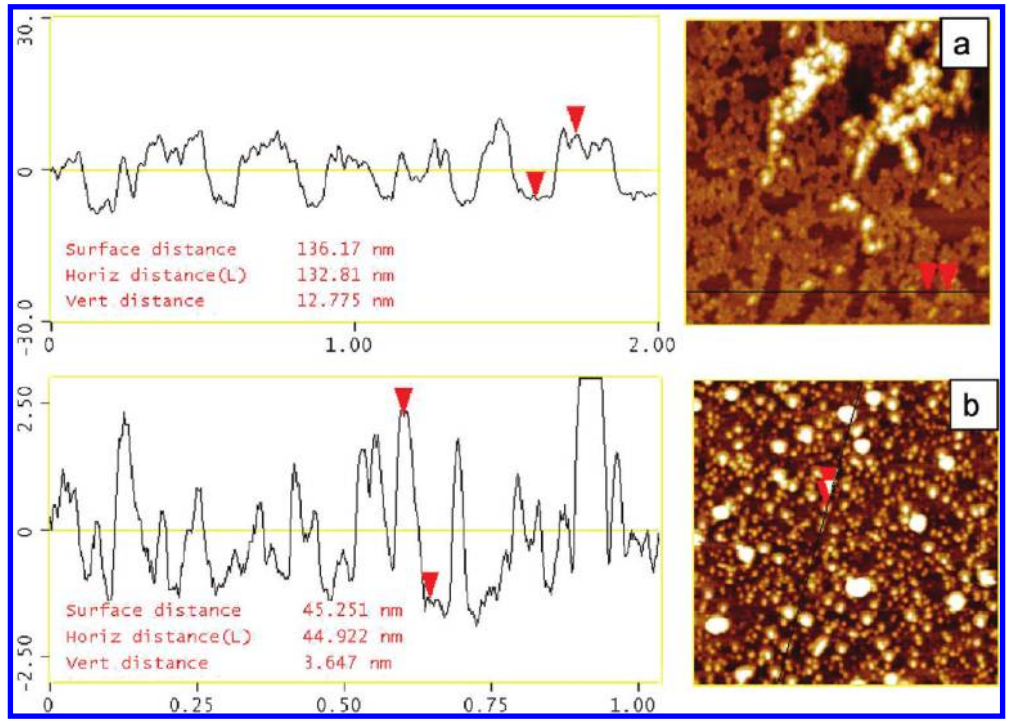

FIGURE 6. Surface topography cross-sections showing the size of titania nanoparticles mineralized on the surface with TiBALDH in (a) water and (b) phosphate citrate buffer solution.

less intense, indicating significant polydispersity in chemical composition due to random polymerization and limited ordering.

Specifically, the peak at 3273 cm^{-1}, indicative of the NH_2 group in the L-histidine, is shifted as nitrogen becomes part of the backbone structure. The amine backbone peak of

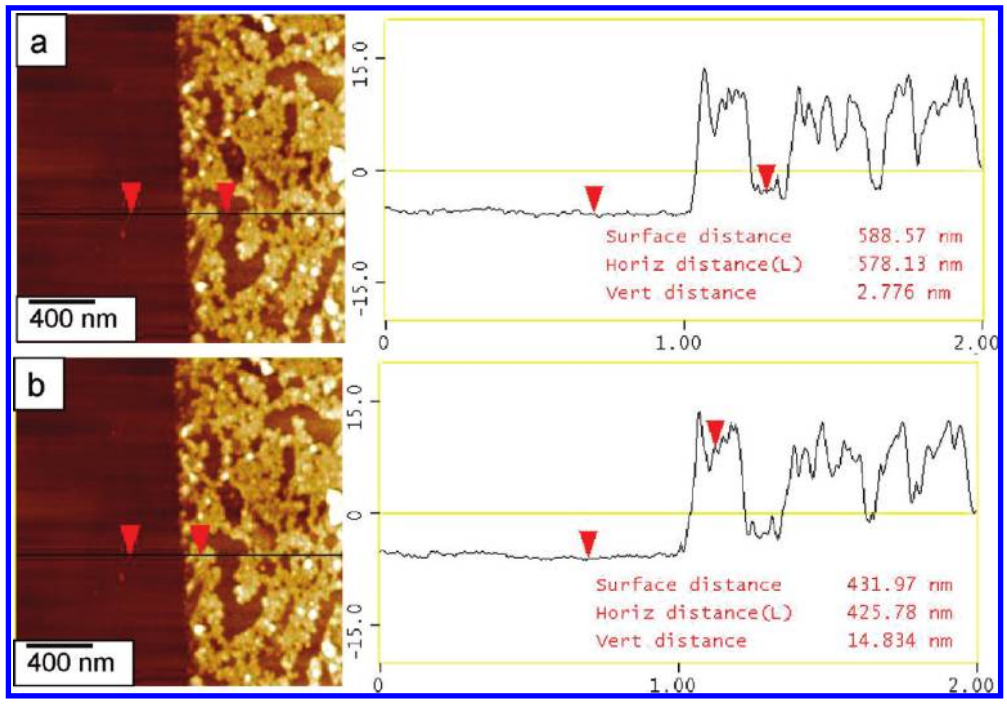

FIGURE 7. AFM scratch test showing the height of (a) the thin residual histidine film present after mineralization on a silicon substrate and (b) the typical particle size in relation to the substrate and residual histidine film. Typical particles sizes ranged from 10−13 nm, as reduced in nanopure water. Topography image, $z = 40$ nm.

polyhistidine is usually reported at 3282 cm^{-1} (61). Also observed is the decrease of peak intensity around 2800 cm^{-1}, indicative of the similar loss of O−H groups during plasma enhanced chemical vapor deposition. This is also affected by the changes in the N−H stretching, as polymerization occurs as well as in the C−H aliphatic stretch mode seen in the L-histidine at 2880 cm^{-1} (62). Strong peaks seen at 1632 and 1608 cm^{-1} indicate C═C, C═O, and C═N bonds and that the ring structure is intact. From these observed changes we can infer that the O−H group is lost and a new bond is formed via the nitrogen, creating the backbone of the polyamino acid network.

Furthermore, the L-histidine shows a strong peak at 1456 cm^{-1} with no peak seen in the plasma-polymerized film at that position. This is likely due to the OH group being removed from the L-histidine during polymerization, as it is present in the L-histidine molecule, but not the linear synthetic polyhistidine material (Scheme 1, Figure 2). Additional peaks seen at 1387, 1361, 1342, 1335, 1110, and 1104 cm^{-1} correspond to the different modes of the C−N, C═N, N−C−H, and C═C bonds present in both the L-histidine and linear polyhistidine (61). The 767 cm^{-1} in the PP-his spectra corresponds to the C═O and N−H in the backbone structure. The 777 cm^{-1} peak in the L-histidine corresponds to the C−C, CH_2, and NH_2 bonds in the intact monomer. From this analysis, we see that the plasma polymerized histidine film is comparable to the L-histidine monomer and corresponding linearly polymerized histidine, with several changes in chemical composition due to random polymerization, but with the retention of essential components of initial monomer unit needed for further titania nanoparticle formation.

The PP-His spectrum is lacking a peak around 1550 cm^{-1}, typically seen in polyhistidine due to C−N bond formation in the backbone (Table 1). This may indicate that there is no clearly defined polymerization occurring, but rather a random network formation of chemical linkages happening between the molecules as they are deposited on the surface.

Titania Nanoparticle Formation. Two different routes were used for the formation of titania nanoparticles on the plasma polymerized histidine surface. The first route used a TiBALDH/water solution (Figure 3a, b) and the second used a TiBALDH/phosphate buffer solution at pH 7 (Figures 4 and 5). Along with a change in topography, the phase images of the particles show a distinct change from that of the plasma deposited thin films, indicating the presence of numerous titania nanoparticles. We observe that there is a high level of titania particle surface coverage measured at approximately 75% in both cases (63, 64). Particle coverage of the surface is typically not seen to be higher than this in part because of the particles not following a close packing regime, as they simultaneously form at many reactive sites on the surface.

Although both routes were successful with mineralization, the primary difference between the two methods was the size of the titania nanoparticles. The diameter for nanoparticles formed in buffer was an average of 3.5 ± 1 nm, while the average diameter of titania nanoparticles obtained from the water-based precursor significantly increased to 13 ± 4 nm (Figure 6). We suggest that this size difference is related to the exposure of an active histidine site in the phosphate buffer. As is known, under different conditions, competitive inhibition occurs differently, which modifies the catalytic activity of the histidine-rich enzymes (65). Additionally, as has been shown, the activity of histidine-serine dipeptides is inhibited by selective interaction with a citrate buffer (66).

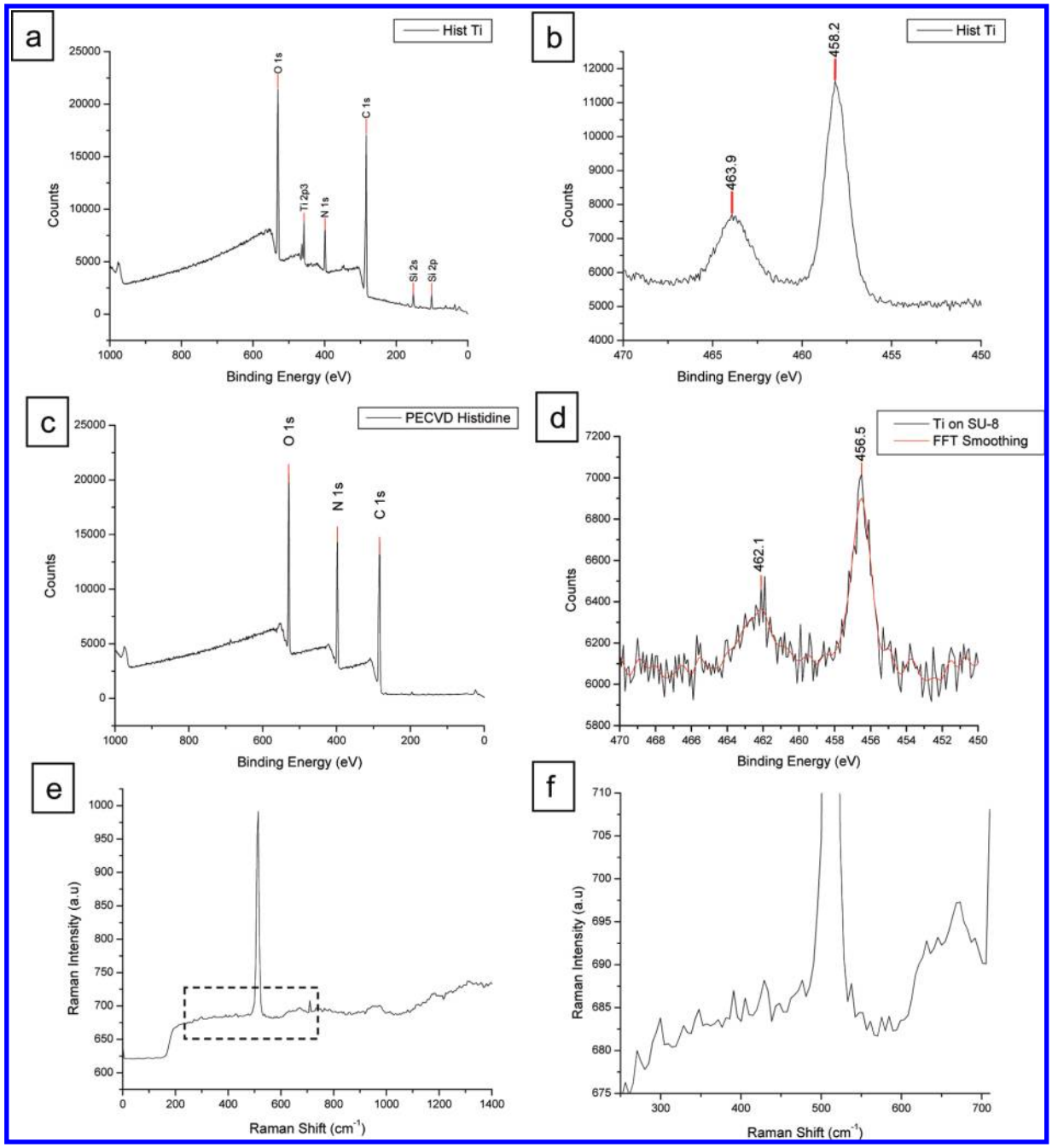

FIGURE 8. XPS spectra of (A) PP-His spectra after titania mineralization; (B) high-resolution XPS scans show distinction between Ti $2p_{1/2}$ and $2p_{3/2}$ for initial PP-His film; (C) XPS spectra of PP-His prior to mineralization; (D) high-resolution spectra of titania mineralized on an SU-8 periodic structure; (E) Raman spectra of mineralized titania on silicon; (F) detailed Raman spectra showing peaks indicative of different titania crystalline phases.

These observations indicate that the phosphate citrate buffer might effectively modify the reactivity of histidine sites available for precursor binding, thus affecting the size of mineralized nanoparticles.

AFM scratch test shows that there are two distinct heights in the final film cross-section after titania nanoparticles formation (Figure 7). We observed that there was a distinct ultrathin residual layer of PP-His under the titania nanoparticles instead of initial histidine film. This layer was typically measured at around 3.5 ± 1 nm. This indicates that during the exposure to the precursor solution, most of the initial PP-His film is dissolved with the exception of an ultrathin surface layer, which remains firmly tethered to the silicon dioxide surface. The PP-His film likely dissolves because of low cross-linking between the molecular chains, which leads to a less-robust structure on the surface.

XPS measurements confirmed the presence of titanium on the histidine surface after exposure to the TiBALDH solution (Figure 8a, 8b). The presence of the characteristic titania peaks are seen in contrast to the pure histidine plasma-deposited film, which shows only carbon, oxygen and nitrogen-related peaks as expected (Figure 8c). Ad-

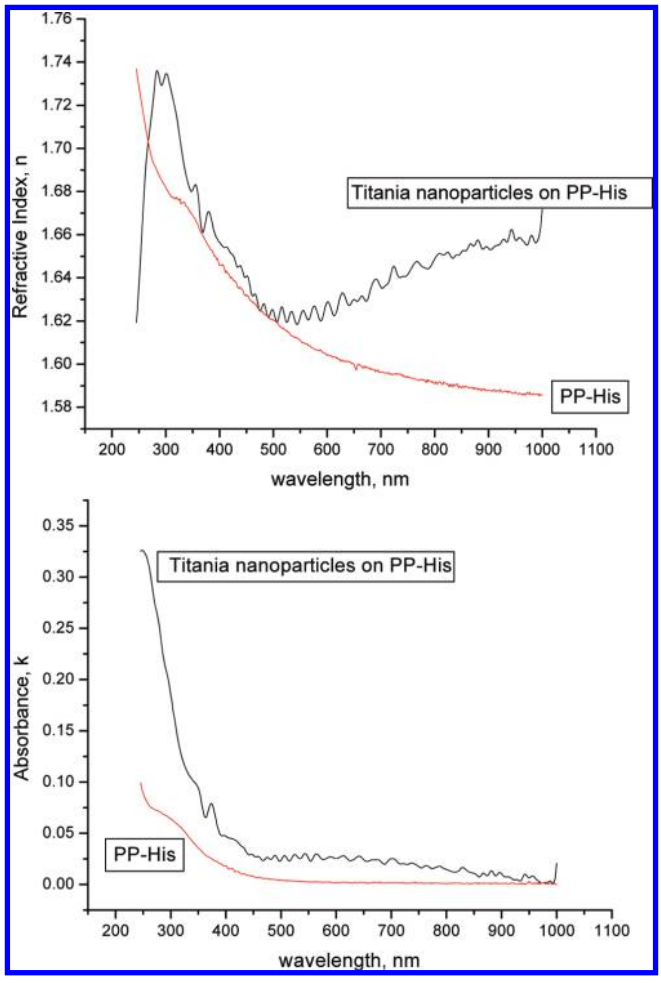

FIGURE 9. Optical analysis from ellipsometric data: refractive index (top) and optical absorbance (bottom) of PP-His film compared to the same with titania nanoparticles.

ditionally, the high resolution XPS spectra show two distinctive peaks of titania, which appear as expected for Ti $2p_{1/2}$ and $2p_{3/2}$ at 463.9 and 458.2, respectively, and agrees well with values previously determined in literature (Figure 8b) (67, 68). A comparison of the observed shape and position of major peaks to those in the literature confirm the presence of titania and indicates that the Ti^{4+} surface species are predominant, as seen by the clear and symmetric peaks (69, 70).

Several attempts to determine the crystal structure of the mineralized titania were made, but the results were inconclusive as to whether there was a definitive crystalline phase. Because the layer of titania was thin (<10 nm) X-ray diffraction measurements could not detect a discernable signal. A second attempt was carried out by plasma depositing histidine on silver particles to perform surface enhanced Raman scattering (SERS) measurements on the subsequently mineralized titania. It is known that Raman spectrum of anatase titania exhibits characteristic bands at 143 cm^{-1} (E_g), 197 cm^{-1}(E_g), 396 cm^{-1} (B_{1g}), 515 cm^{-1} (A_{1g} or B_{1g}), and 638 cm^{-1} (E_g). For rutile titania, Raman bands from are located at 439 cm^{-1} (E_g), 611 cm^{-1} (A_{1g}), and 805 cm^{-1} (a weak shoulder, B_{1g}) (71, 72). The Raman spectra obtained here showed several peaks that could be indicative of either rutile (440 and 230 cm^{-1}) or the brookite (405 and 630 cm^{-1}) phases of titania (Figure 8e, f). Therefore, it remains open as to which phase is dominant via this mineralization technique, and mixed structures are probably formed under these conditions.

Optical Properties of Films. A direct determination of the optical properties of aminoacid and titania-containing films was obtained by exploiting a bi-layered model during analysis of spectroscopic ellipsometry data. At least six individual samples were fabricated under identical conditions and were independently measured and analyzed. Ellipsometric measurements were conducted for the polymerized histidine film and for the histidine film with the topmost titania layer. For full analysis of the titania-containing films, independently measured optical properties of the pure PP-His film were utilized. Since AFM measurements indicated that the titania nanoparticle layer showed only partial surface coverage, an effective medium approximation was used to model this layer. The two models used in determining the optical constants were the Cauchy and effective medium approximation (EMA). Both models produced consistent and reliable results (45, 63). The EMA model was used to verify the results of the Cauchy model because the layer of titania particles was not complete and included some small voids, which can be effectively accounted for when using EMA analysis.

The values for the thicknesses of the PP-His and titania layers determined from ellipsometry closely matched those measured by AFM which was considered as verification of the optical analysis routine. The optical constants n and k over a wide wavelength range are presented in Figure 9. The intact PP-histidine films showed a normal dispersion with a gradually decreasing refractive index, n, from 1.68 at 350 nm down to 1.59 in the near-IR region (1000 nm) (Figure 9). The minor shoulder around 300 nm is caused by the strong absorption of double bonds in the histidine structure (Figure 1). The overall level of refractive index is slightly higher than that for traditional polymers (usually within 1.5−1.6), likely because of the higher concentration of cross-linkings and packing density in plasma polymerized film that result from the network formation (73). On the other hand, the absorption coefficient, k, is relatively high in near-UV range because of the presence of double bonds and ring structure. But the k-value decreased to below 2×10^{-3} in the visible and near-IR range, indicating low light absorption and good optical transparency in comparison to conventional, covalently cross-linked polymers with localized ordering (74).

A significant increase in the refractive index value is observed upon titania nanoparticle formations in the entire wavelength range (Figure 9). The refractive index increased to 1.74 from 1.67 in the UV region and to near 1.65 at 1000 nm which is within 0.05−0.08 at different wavelengths. The titania nanoparticle formation also increased the optical absorbance to 0.025 in the visible range, indicating some optical loss likely due to additional scattering by densely

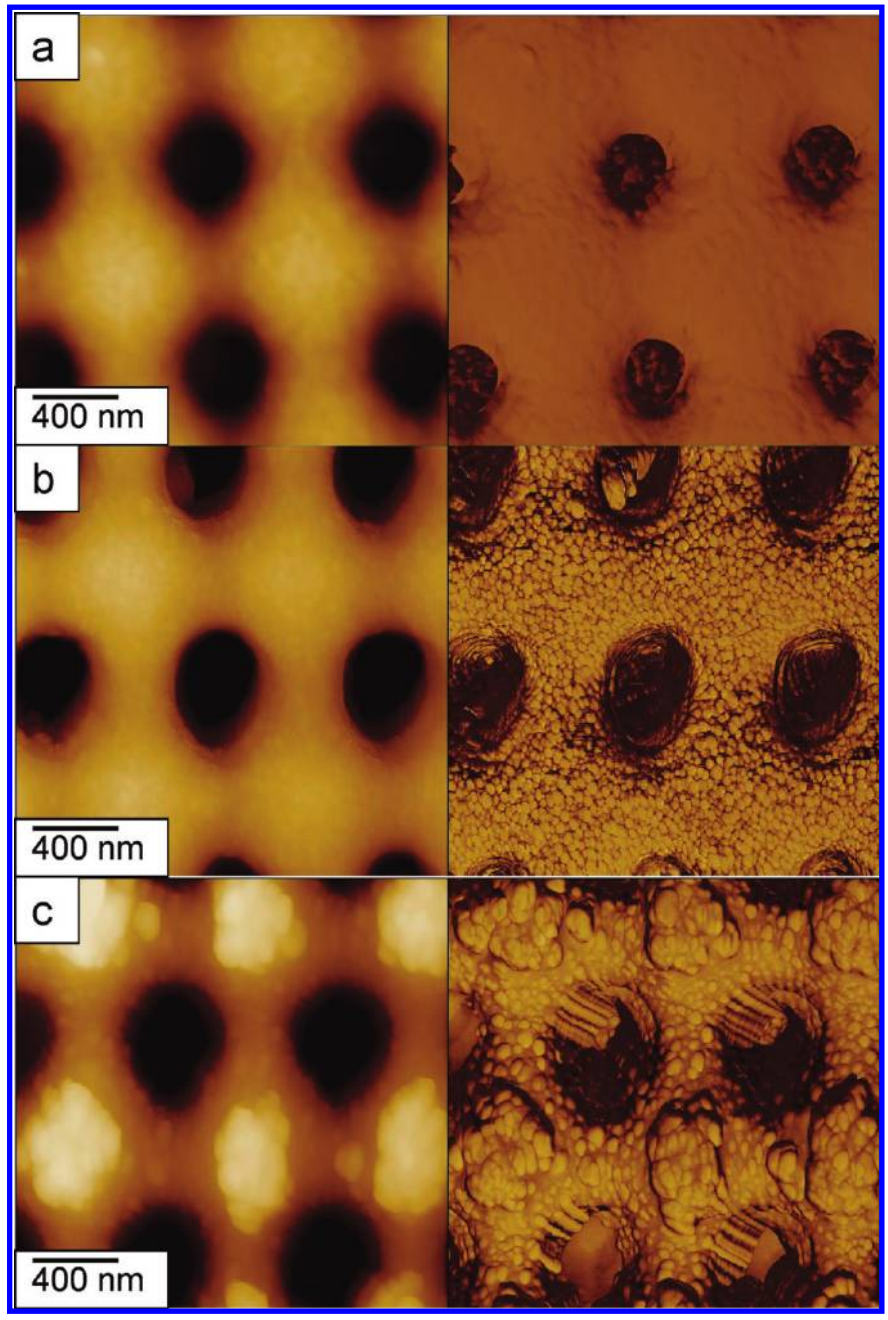

FIGURE 10. AFM images demonstrating the conformal titania nanocoatings on periodic porous structure (topography, left; phase, right; all images): (A) pristine periodic structure before modification, $z = 300$ nm height and 170° phase; (B) periodic structure after one PP-his polymerization and titania formation showing significant change in the phase image, $z = 500$ nm height and 40° phase; (C) periodic structure after three titania formation cycles. Large agglomerations of particles are easily visible on nodes, $z = 600$ nm height and 60° phase.

packed surface layer of titania nanoparticles and their aggregates (Figure 9).

Although the measured value of the refractive index increased significantly due to the presence of titania nanoparticles, it is still much lower than that of crystalline titania phases (about 2.7 at $\lambda = 500$ nm) (75–77). For example, the reported literature values for the atomic layer deposited (ALD) titania range from about 2.3 to 2.8 at $\lambda = 500$ nm, depending on the deposition conditions (78, 79). However, for titania films of less than 20 nm thickness, the refractive index was reported to be 1.8 at 500 nm, which was significantly lower than the index of thicker titania films, thus demonstrating a trend similar to that observed for reduced refractive index for ultrathin titania layer without further high-temperature annealing (80).

Finally, we suggest that the measured refractive index of the titania nanoparticles formed on biosurface appears lower for two primary reasons. First, the titania nanoparticle layer is incomplete, having both voids and organic matter between the nanoparticles that contribute to the lowering of the refractive index even within EMA analysis which is not accounted for by current modeling. Titania nanoparticles formed via a bioenabled wet-chemistry approach typically show an amorphous phase that has a characteristically lower

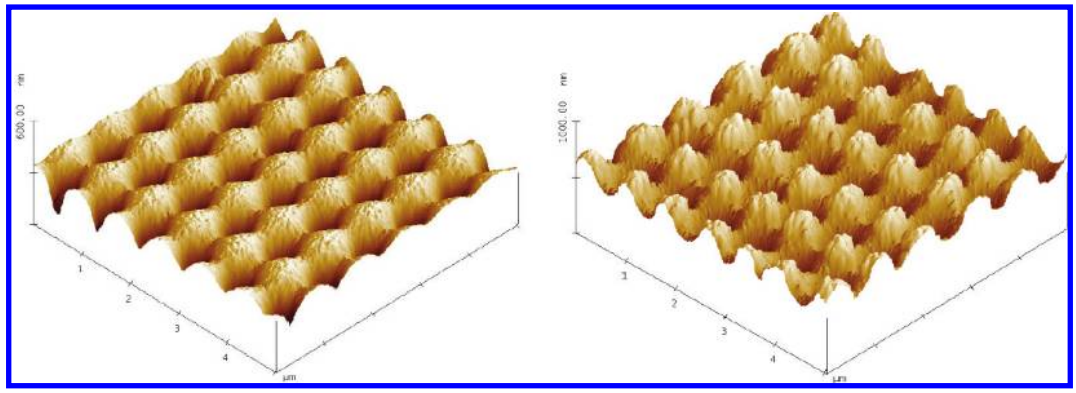

FIGURE 11. 3D AFM (topography) images at large scale showing pristine squared periodic porous pattern (left) $z = 600$ nm height and the same structure after titania nanoparticle formation on lattice nodes (right), $z = 1000$ nm height.

refractive index than common crystalline titania phases, which have proven to be difficult to obtain using room temperature synthesis routines (81). Additional treatment of titania phase and increasing surface coverage might be required to boost the absolute values of the refractive index for potential high refractive properties. However, even for the values observed here, a significant contrast in refractive indices can be achieved in the visible range if the titania layer is combined with low index polymer materials.

Titania Formation on Periodic 3D Templates. Periodic photonic structures with a square lattice of cylindrical pores of periodic spacing 830 nm served here as the basic template to demonstrate the highly conformal nature of such depositions (82). Prior to the plasma depositions and subsequent particle formation, the surface morphology was observed to be clean and free of defects or nodes, seen after mineralization (Figure 10a). Plasma polymerization of histidine and the following formation of titania in pre-cursor solution resulted in a visible change in the surface morphology (Figure 10b). The AFM images clearly demonstrate the highly conformal nature and uniformity of PP-histidine nanocoating as evidenced by uniformly distributed presence of titania nanoparticles over the surface of periodic structures. The surface coverage with titania nanoparticles can be increased by repeated exposure to precursor solution with titania nanoparticles showing a trend for significant agglomeration after multiple treatment cycles as demonstrated in the corresponding AFM images of such specimens (Figure 10c).

The titania-coated structures exhibit the same periodic pattern over a larger surface area with a very repeatable local morphology of the polymeric nodes (Figure 11). Local microroughness of these nodes after histidine polymerization indicates the presence of the additional plasma coating. Although the square pattern of nodes remains unchanged after titania formation, local morphology of nodes changed significantly because of the presence of the titania nanoparticles localized at nodes of the squared lattice.

CONCLUSIONS

We demonstrate the implementation of plasma-deposited amino acids as functional surface coatings for the conformal formation of titania nanoparticles. This is a rapid and non-destructive method for the formation of a functional histidine layer which can then be utilized for forming individual and uniform titania nanoparticles under mild, environmentally friendly conditions enabling the modification of the surface properties of original templates. These titania nanoparticles possessing higher refractive index were demonstrated on both smooth substrates and on complex 3D periodic porous polymers such as IL structures. This coating and in situ titania growth may be useful in the creation of high-contrast periodic photonic-related structures formed under mild conditions. By directly reducing the titania onto or into a prefabricated periodic porous structure, this approach might allow full construction of a hybrid organic−inorganic system to be fabricated.

This type of bioenabled modification highlights a very interesting technique which can be used to modify these structures and warrant further study into their optical and catalytic properties. For instance, the periodic polymeric structures are prone to mechanical instabilities even under moderate compressive stresses (83, 84). Under mild processing conditions suggested in this study, there was no degradation and collapse in the periodic polymer structure. By creating a method to embed titania nanostructures onto periodic polymer templates, we demonstrate a means of tailoring photonic structures and their refractive properties in nondestructive way. This approach can also be used in stepwise construction of multilayered systems where the PP-His layer alternates with polymer layer, thus creating high contrast in refractive index variation. Further development of the optical and catalytic properties of the titania replicas obtained here will be addressed in our future investigations.

Acknowledgment. This work is supported by the Air Office of Scientific Research FA9550-08-1-0446 and FA9550-09-1-0162 Projects and Air Force Research Lab and the NDSEG Fellowship (K.A.). The authors thank Dr. Ray Gunawidjaja and Dr. Kurt Eyink (WPAFB) for technical assistance with ellipsometry, Dr. Matthew Dickerson (WPAFB) for useful discussions, and Prof. E. L. Thomas' group at MIT for providing the IL structures.

REFERENCES AND NOTES

(1) Jeffryes, C.; Gutu, T.; Jiao, J.; Rorrer, G. L. *J. Mater. Res.* **2008**, *23*, 3255. Koberstein, J. T. *J. Polym. Sci.,Part B: Polym. Phys.* **2004**, *42*, 2942. Crowe, J. A.; Genzer, J. C. *J. Am. Chem. Soc.* **2005**, *127*, 17610.

(2) Mendes, P. M. *Chem. Soc. Rev.* **2008**, *37*, 2512.

(3) Senaratne, W.; Andruzzi, L.; Ober, C. K. *Biomacromolecules* **2005**, *6*, 2427.

(4) Tokarev, I.; Tokareva, I.; Minko, S. *Adv Mater.* **2008**, *20*, 2730. Urban, M. W. *Polym. Rev.* **2006**, *46*, 329. Andreeva, D.V.; Fix, D.; Mohwald, H.; Shchukin, D. G. *Adv. Mater.* **2008**, *20*, 2789. Russel, T.P. *Science* **2002**, *297*, 964.

(5) Tsukruk, V. V. *Adv. Mater.* **2001**, *13*, 95. Singamaneni, S.; McConney, M. E.; LeMieux, M. C.; Jiang, H.; Enlow, J. O.; Bunning, T. J.; Naik, R. R.; Tsukruk, V. V. *Adv. Mater.* **2007**, *19*, 4248. Julthongpiput, D.; Lin, Y.-H.; Teng, J.; Zubarev, E. R.; Tsukruk, V. V. *J. Am. Chem. Soc.* **2003**, *125*, 15912.

(6) Horváth, A.; Beck, A.; Sárkány, A.; Stefler, G.; Varga, Z.; Geszti, O.; Tóth, L.; Guczi, L. *J. Phys. Chem. B* **2006**, *110*, 15417.

(7) Bertino, M. F.; Smarsly, B.; Stocco, A.; Stark, A. *Adv. Funct. Mater.* **2009**, *19*, 1235.

(8) Stuart, M. C.; Huck, W.; Genzer, J.; Müller, M.; Ober, C.; Stamm, M.; Sukhorukov, G.; Szleifer, I.; Tsukruk, V. V.; Urban, M.; Winnik, F.; Zauscher, S.; Luzinov, I.; Minko, S. *Nat. Mater.* **2010**, *9*, 101.

(9) Luzinov, I.; Minko, S.; Tsukruk, V. V. *Soft Matter* **2008**, *4*, 714. Luzinov, I.; Minko, S.; Tsukruk, V. V. *Prog. Polym. Sci.* **2004**, *29*, 635.

(10) Jin, R.-H.; Yuan, J.-J. *Adv. Mater.* **2009**, *21*, 3750.

(11) Klem, M. T.; Young, M.; Douglas, T. *J. Mater. Chem.* **2008**, *18*, 3821.

(12) Singamaneni, S.; Kharlampieva, E.; Jang, J.-H.; McConney, M. E.; Jiang, H.; Bunning, T. J.; Thomas, E. L.; Tsukruk, V. V. *Adv. Mater.* **2010**, *22*, 1369. Kharlampieva, E.; Slocik, J. M.; Singamaneni, S.; Poulsen, N.; Kröger, N.; Naik, R. R.; Tsukruk, V. V. *Adv. Funct. Mater.* **2009**, *19*, 2303.

(13) Kozlovskaya, V.; Kharlampieva, E.; Chang, S.; Muhlbauer, R.; Tsukruk, V. V. *Chem. Mater.* **2009**, *21*, 2158. Kharlampieva, E.; Slocik, J. M.; Singamaneni, S.; Poulsen, N.; Kroger, N.; Naik, R. R.; Tsukruk, V. V. *Adv. Funct. Mater.* **2009**, *19*, 2303.

(14) Kozlovskaya, V.; Kharlampieva, E.; Khanal, B. P.; Manna, P.; Zubarev, E. R.; Tsukruk, V. V. *Chem. Mater.* **2008**, *20*, 7474.

(15) Dickerson, M. B.; Sandhage, K. H.; Naik, R. R. *Chem. Rev.* **2008**, *108*, 4935.

(16) Durupthy, O.; Bill, J.; Aldinger, F. *Cryst. Growth Des.* **2007**, *7*, 2696.

(17) Zhao, Y.; Pérez-Segarra, W.; Shi, Q.; Wei, A. *J. Am. Chem. Soc.* **2005**, *127*, 7328.

(18) Dubois, F.; Mahler, B.; Dubertret, B.; Doris, E.; Mioskowski, C. *J. Am. Chem Soc.* **2007**, *129*, 482.

(19) Yuan, J.-J.; Jin, R.-H. *Langmuir* **2010**, *26*, 4212.

(20) Sano, K.-I.; Yoshii, S.; Yamashita, I.; Shiba, K. *Nano Lett.* **2007**, *7*, 3201.

(21) Rybak, B. M.; Bergman, K. N.; Ornatska, M.; Genson, K. L.; Tsukruk, V. V. *Langmuir* **2006**, *22*, 1027.

(22) Jin, R. H.; Yuan, J. J. *J. Mater. Chem.* **2005**, *15*, 4513.

(23) Daniel, M. C.; Astruc, D. *Chem. Rev.* **2004**, *104*, 293.

(24) Naik, R. R.; Stringer, S. J.; Agarwal, G.; Jones, S. E.; Stone, M. O. *Nat. Mater.* **2002**, *1*, 169.

(25) Si, S.; Mandal, T. K. *Chem.—Eur. J.* **2007**, *13*, 3160.

(26) Dujardin, E.; Peet, C. l.; Stubbs, G.; Culver, J. N.; Mann, S. *Nano Lett.* **2003**, *3*, 413.

(27) Mann, S. *Biomineralization: Principles and Concepts in Bioinorganic Materials Chemistry*; Oxford University Press: Oxford, U.K., 2001.

(28) Dickerson, M. B.; Jones, S. E.; Cai, Y.; Ahmad, G.; Naik, R. R.; Kröger, N.; Sandhage, K. H. *Chem. Mater.* **2008**, *20*, 1578.

(29) Slocik, J. M.; Moore, J. T.; Wright, D. W. *Nano Lett.* **2002**, *2*, 169.

(30) Tahir, M. N.; Théato, P.; Müller, W. E. G.; Schröder, H. C.; Borejko, A.; Faiβ, S.; Janshoff, A.; Huth, J.; Tremel, W. *Chem. Commun.* **2005**, 5533.

(31) Yang, S. H.; Kang, K.; Choi, I. S. *Chem. Asian. J.* **2008**, *3*, 2097.

(32) Wang, J.; Xu, J.; Goodman, M. D.; Chen, Y.; Cai, M.; Shinar, J.; Lin, Z. *J. Mater. Chem.* **2008**, *18*, 3270.

(33) Kröger, N.; Dickerson, M. B.; Ahmad, G.; Cai, Y.; Haluska, M. S.; Sandhage, K. H.; Poulsen, N.; Sheppard, V. C. *Angew. Chem., Int. Ed.* **2006**, *45*, 7239.

(34) Kharlampieva, E.; Tsukruk, T.; Slocik, J. M.; Ko, H. H.; Poulsen, N.; Naik, R. R.; Kröger, N.; Tsrukruk, V. V. *Adv. Mater.* **2008**, *20*, 3274.

(35) Karaman, M.; Kooi, S. E.; Gleason, K. K. *Chem. Mater.* **2008**, *20*, 2262.

(36) Bonifacio, L. D.; Lotsch, B. V.; Puzzo, D. P.; Scotognella, F.; Ozin, G. A. *Adv. Mater.* **2009**, *21*, 1641.

(37) Puzzo, D. P.; Bonifacio, L. D.; Oreopoulos, J.; Yip, C. M.; Manners, I.; Ozin, G. A. *J. Mater. Chem.* **2009**, *19*, 3500.

(38) Hidalgo, N.; Calvo, M. E.; Míguez, H. *Small* **2009**, *5*, 2309.

(39) Kang, Y.; Walish, J. J.; Gorishnyy, T.; Thomas, E. L. *Nat. Mater.* **2007**, *6*, 957.

(40) King, J. S.; Graugnard, E.; Roche, O. M.; Sharp, D. N.; Scrimgeour, J.; Denning, R. G.; Turberfield, A. J.; Summers, C. *J. Adv. Mater.* **2006**, *18*, 1561.

(41) Moon, J. H.; Yang, S.; Dong, W. T.; Perry, J. W.; Adibi, A.; Yang, S. M. *Opt. Express* **2006**, *14*, 6297.

(42) Xu, Y.; Zhu, X.; Dan, Y.; Moon, J. H.; Chen, V. W.; Johnson, A. T.; Perry, J. W.; Yang, S. *Chem. Mater.* **2008**, *20*, 1816.

(43) Yasuda, H. *Plasma Polymerization*; Academic Press: New York, 1985.

(44) Sreenivasan, R.; Gleason, K. K. *Chem. Vap. Deposition* **2009**, *15*, 77.

(45) Martinu, L.; Poitras, D. *J. Vac. Sci. Technol., A* **2000**, *18*, 2619.

(46) Anderson, K. D.; Slocik, J. M.; McConney, M. E.; Enlow, J. O.; Jakubiak, R.; Bunning, T. J.; Naik, R. R.; Tsukruk, V. V. *Small* **2009**, *5*, 741.

(47) Singamaneni, S.; LeMieux, M. C.; Jiang, H.; Bunning, T. J.; Tsukruk, V.V. *Chem. Mater.* **2007**, *19*, 129.

(48) Maldovan, M.; Thomas, E. L. *Periodic Materials and Interference Lithography: For Photonics, Phononics and Mechanics*; Wiley-VCH: Weinheim, Germany, 2008.

(49) Ullal, C. K.; Maldovan, M.; Thomas, E. L.; Chen, G.; Han, Y.-J.; Yang, S. *Appl. Phys. Lett.* **2004**, *84*, 5434.

(50) Moon, J. H.; Ford, J.; Yang, S. *Polym. Adv. Technol.* **2006**, *17*, 83.

(51) LeMieux, M. C.; McConney, M. E.; Lin, Y.-H.; Singamaneni, S.; Jiang, H.; Bunning, T. J.; Tsukruk, V. V. *Nano Lett.* **2006**, *6*, 730.

(52) Enlow, J. O.; Jiang, H.; Grant, J. T.; Eyink, K.; Su, W.; Bunning, T. J. *Polymer* **2008**, *49*, 4042.

(53) Choi, T.; Jang, J.-H.; Ullal, C. K.; Lemieux, M. C.; Tsukruk, V. V.; Thomas, E. L. *Adv. Funct. Mater.* **2006**, *16*, 1324.

(54) Jang, J.-H.; Ullal, C. K.; Maldovan, M.; Gorishnyy, T.; Kooi, S.; Koh, C. Y.; Thomas, E. L. *Adv. Funct. Mater.* **2007**, *17*, 3027.

(55) Tsukruk, V. V.; Reneker, D. H. *Polymer* **1995**, *36*, 1791.

(56) Tsukruk, V. V. *Rubber Chem. Technol.* **1997**, *70*, 430.

(57) McConney, M. E. Singamaneni, S. Tsukruk, V. V. *Polym. Rev.* **2010**, doi:10.1080/15583724.2010.493255.

(58) Dammak, T.; Fourati, N.; Abid, Y.; Boughzala, H.; Mlayah, A.; Minot, C. *Spectrochim. Acta, A* **2007**, *66*, 1097.

(59) Madhavan, J.; Aruna, S.; Anuradha, A.; Premanand, D.; Potheher, I. V.; Thamizharasan, K.; Sagayaraj, P. *Opt. Mater.* **2007**, *29*, 1211.

(60) Wolpert, M.; Hellwig, P. *Spectrochim. Acta, A* **2006**, *64*, 987.

(61) La'verne, S. J.; Srivastave, S.; Srivastave, S.; Srivastave, S.; Gupta, V. D. *J. Polym. Sci., Polym. Phys.* **2010**, *48*, 128.

(62) Madhavan, J.; Aruna, S.; Thomas, P.C.; Vimalan, M.; Rajasekar, S. A.; Sagayaraj, P. *Cryst. Res. Technol.* **2007**, *42*, 59.

(63) Tompkins, H. G.; Irene, E. A. *Handbook of Ellipsometry*; Springer Science & Business: New York, 2005; p 60.

(64) Roussel, P. J.; Vanhellemont, J.; Maes, H. E. *Thin Solid Films* **1993**, *234*, 423.

(65) Krajewska, B.; Zaborska, W. *J. Mol. Catal., B* **1999**, *6*, 75.

(66) Sun, M.; Chen, J.; Liu, X. H.; Zhao, Y. F. *J. Mol. Struct.—Theochem* **2004**, *668*, 47.

(67) Jensen, H.; Soloviev, A.; Li, Z.; Søgaard, R. G. *Appl. Surf. Sci.* **2005**, *246*, 239.

(68) Greenlief, C. M.; White, J. M.; Ko, C. S.; Gorte, R. J. *J. Phys. Chem.* **1985**, *89*, 5025.

(69) Jing, L.; Sun, X.; Cai, W.; Xu, Z.; Du, Y.; Fu, H. *J. Phys. Chem. Solids* **2003**, *64*, 615.

(70) Rahman, M. M.; Krishna, K. M.; Soga, T.; Jimbo, T.; Umeno, M. *J. Phys. Chem. Solids* **1999**, *60*, 201.

(71) Ocana, M.; Garcia-Ramos, J.V.; Serna, C.J. *J. Am. Ceram. Soc.* **1992**, *75*, 2010.

(72) Robert, T. D.; Laude, L. D.; Geskin, V. M.; Lazzaroni, R.; Gouttebaron, R. *Thin Solid Films* **2003**, *440*, 268.

(73) Kasarova, S. N.; Sultanova, N. G.; Ivanov, C. D.; Nikolov, I. D. *Opt. Mater.* **2007**, *29*, 1481.

(74) (a) Crews, P.; Rodríguez, J.; Jaspars, M. *Organic Structure Analysis*; Oxford University Press: New York, 1998. (b) Pretsch, E.; Bühlmann, P.; Affolter, C. *Structure Determination of Organic Compounds*; Springer: Berlin, 2000.
(75) Sbai, N.; Perrière, J.; Gallas, B.; Millon, E.; Seiler, W.; Bernard, M. C. *J. Appl. Phys.* **2009**, *104*, 033529.
(76) Abaffy, N. B.; Evans, P.; Triani, G.; McCulloch, D. *Proc. SPIE* **2008**, *7041*, 704109.
(77) Bendavid, A.; Martin, P. J.; Preston, E. W. *Thin Solid Films* **2008**, *517*, 494.
(78) Jiang, H.-Q.; Wei, Q.; Cao, Q.-X.; Yao, X. *Ceram. Int.* **2008**, *34*, 1039.
(79) Aarik, J.; Aidla, A.; Mändar, H.; Uustare, T.; Schuisky, M.; Hårsta, A. *J. Cryst. Growth* **2002**, *242*, 189.
(80) Kasikov, A.; Aarik, J.; Mändar, H.; Moppel, M.; Pärs, M.; Uustare, T. *J. Phys. D: Appl. Phys.* **2006**, *39*, 54.
(81) Aarik, J.; Aidla, A.; Kiisler, A.-A.; Uustare, T.; Sammelselg, V. *Thin Solid Films* **1997**, *305*, 270.
(82) Singamaneni, S.; Chang, S.; Jang, J.-H.; Davis, W.; Thomas, E. L.; Tsukruk, V. V. *Phys. Chem. Chem. Phys* **2008**, *10*, 4093.
(83) Singamaneni, S.; Bertoldi, K.; Chang, S.; Jang, J. H.; Thomas, E. L.; Boyce, M.; Tsukruk, V. V. *Adv. Funct. Mater.* **2009**, *19*, 1426.
(84) Singamaneni, S.; Bertoldi, K.; Chang, S.; Jang, J. H.; Thomas, E. L.; Boyce, M.; Tsukruk, V. V. *ACS. Appl. Mater. Interfaces* **2009**, *1*, 42.

AM1003365